PHYSICAL REVIEW D VOLUME 42, NUMBER 5 1 SEPTEMBER 1990

Measurement of the two-photon width of the $\eta'(958)$

F. Butler,[a] J. Boyer,[b] G. Gidal, G. Abrams, D. Amidei,[c] A. R. Baden,[d] M. S. Gold,
G. Goldhaber, L. Golding,[e] J. Haggerty,[f] D. Herrup,[g] I. Juricic,[b] J. A. Kadyk,
M. E. Levi, M. E. Nelson,[h] P. C. Rowson,[b] H. Schellman,[g] W. B. Schmidke,
P. D. Sheldon,[i] G. H. Trilling, and D. R. Wood[j]
Lawrence Berkeley Laboratory and Department of Physics, University of California, Berkeley, California 94720

K. Riles, M. L. Perl, T. Barklow, A. Boyarski, P. R. Burchat,[k] D. L. Burke,
J. M. Dorfan, G. J. Feldman, L. Gladney,[l] G. Hanson, K. Hayes, R. J. Hollebeek,[l]
W. R. Innes, J. A. Jaros, D. Karlen,[m] S. R. Klein, A. J. Lankford, R. R. Larsen,
B. W. LeClaire,[j] N. S. Lockyer,[l] V. Lüth, R. A. Ong,[c] B. Richter, and J. M. Yelton[n]
Stanford Linear Accelerator Center, Stanford University, Stanford, California 94305

T. Schaad[p]
Department of Physics, Harvard University, Cambridge, Massachusetts 02138
(Received 27 March 1990)

Using 203 pb^{-1} of data collected by the Mark II detector at the SLAC storage ring PEP, we have measured the radiative width of the η' for quasireal photons. The width is separately measured in the three reactions $e^+e^-\to e^+e^-\eta^0\pi^+\pi^-$, $\eta^0\to\gamma\gamma$; $e^+e^-\to e^+e^-\eta^0\pi^+\pi^-$; $\eta^0\to\pi^+\pi^-(\pi^0,\gamma)$; and $e^+e^-\to e^+e^-\rho^0\gamma$, giving a statistically weighted average two-photon width of $\Gamma_{\eta'\to\gamma\gamma}=4.57\pm0.25\pm0.44$ keV. As a byproduct of the study of the decay mode $\eta'\to\rho\gamma$, we also measured the two-photon decay width of the $a_2(1320)$ as $\Gamma_{a_2(1320)\to\gamma\gamma}=1.03\pm0.13\pm0.21$ keV.

The measurement of the two-photon widths of the $C=+$ pseudoscalar mesons can be used to simultaneously measure the octet-singlet mixing angle Θ and to probe the charged-parton content of these mesons. Early measurements have shown inconsistencies both internally and with measurements made in hadronic production. Possible gluonium admixtures in the η and η' mesons can also alter the mixing between these states.

The first measurement of the two-photon width of the η' was made with the Mark II detector at the SLAC e^+e^- storage ring SPEAR and gave a value of $5.8\pm1.1\pm1.2$ keV using the $\rho^0\gamma$ decay mode.[1] More recent measurements,[2–10] using primarily the same decay mode, have given smaller values, so that the current world average stands at $\Gamma(\eta'\to\gamma\gamma)=4.20\pm0.09$ keV.

We report the results of three independent measurements[11] of the η' radiative width, $\Gamma(\eta'\to\gamma\gamma)$, with the Mark II detector at the SLAC e^+e^- storage ring PEP operating at $E_{\mathrm{c.m.}}=29$ GeV. The reactions used detect three distinct η' decay modes:

$$e^+e^-\to e^+e^-\eta';\eta'\to\rho^0\gamma\ , \tag{1}$$

$$e^+e^-\to e^+e^-\eta';\eta'\to\eta\pi^+\pi^-;\eta\to\gamma\gamma\ , \tag{2}$$

$$e^+e^-\to e^+e^-\eta';\eta'\to\eta\pi^+\pi^-;\eta\to\pi^+\pi^-(\pi^0,\gamma)\ . \tag{3}$$

The detector and trigger are described in Sec. I. Section II describes the data processing and the Monte Carlo simulation. Sections III–V are then devoted to the analysis of reactions (1)–(3), with the implications and conclusions given in Sec. VI.

I. DETECTOR AND TRIGGER

The Mark II at PEP [see Figs. 1(a) and 1(b)] was a general-purpose magnetic spectrometer designed to detect the charged and neutral particles resulting from high-energy e^+e^- annihilation and the collision of virtual photons associated with the electromagnetic fields surrounding the positrons and electrons. In the central two thirds of the solid angle there are drift chambers for precision tracking and momentum determination, a time-of-flight (TOF) system for limited particle identification, a liquid-argon electromagnetic calorimeter for electron and photon identification, and four layers of steel and proportional tubes for muon identification. In addition, at smaller polar angles there are lead proportional chamber end caps and a small-angle-tagger (SAT) system used for identifying very small angle electrons and for luminosity determination. The main features of the detector have been previously described.[12]

The Mark II was moved to PEP from the SPEAR e^+e^- storage ring at the Stanford Linear Accelerator Center (SLAC). During the Mark II's history at PEP, several detector configurations were used. We will be using only data collected after the magnetic-field strength was reduced to 2.35 kG due to the loss of one magnet coil. A total of approximately 203 pb^{-1} of data at a center-of-mass energy of 29 GeV were collected at PEP in this configuration. The rather low field in combination with the precision tracking, made possible by the vertex chamber and the use of a 1.4-mm-thick beryllium beam pipe, permitted us to accurately measure the low-momentum tracks characteristic of reactions (1)–(3).

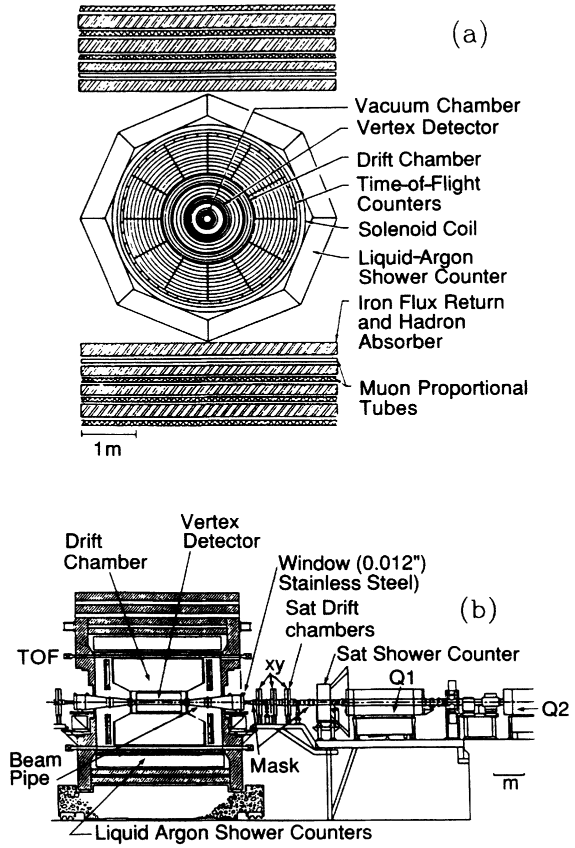

FIG. 1. (a) The Mark II detector viewed along the beam axis, and (b) an isometric view of the detector.

The beam crossing rate at PEP of approximately 400 kHz necessitated a selective electronic trigger system, and the Mark II two-level trigger was able to hold the event acquisition rate to a few Hertz. The principle employed combined a fast (≈ 1 μsec) and relatively simple primary trigger, with a more sophisticated pattern-recognizing secondary trigger that used data from the two drift chambers to find charged tracks. A master interrupt controller (MIC) orchestrated the two-tiered system.

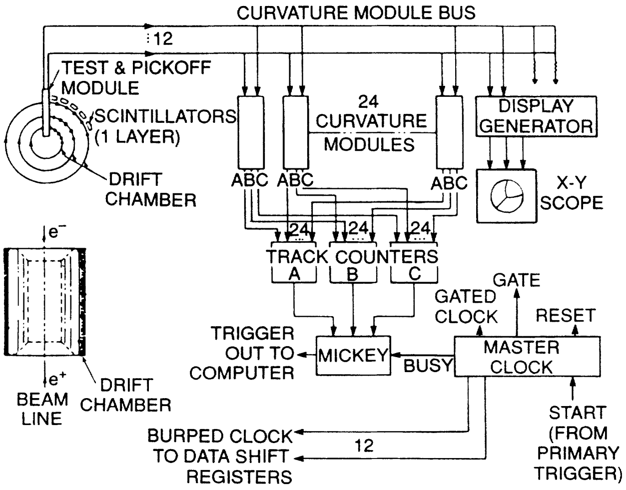

FIG. 2. A block diagram of the secondary trigger system.

Various primary triggers were employed. The coincidence of a delayed beam crossing signal with a TOF hit signal and the satisfaction of a drift-chamber and vertex-chamber layer hit pattern criterion defined a track. The events used in this analysis typically satisfied the "charged trigger" which required that at least two such tracks were found by the pattern-recognition hardware. Since the trigger efficiency for low-momentum charged particles is such an important component of our results, we discuss the trigger in some detail in the Appendix. (See Fig. 2.) The "neutral trigger" fired if a threshold was exceeded in the front section of any two of the eight liquid-argon calorimeter modules, or if the total calorimetric energy deposit (including the end-cap proportional-tube calorimeters) exceeded a higher threshold. A scaled "Bhabha trigger" used the SAT system to trigger on small-angle Bhabha scattering events.

II. DATA PROCESSING AND EVENT SIMULATION

A. Two-photon-event summary tapes

For a large part of the data it was necessary to reverse the effects of a subroutine added to the normal tracking program (PASS2) to help reduce the use of computer time. Raw events which had previously been discarded were selected if the trigger hardware found one or more (noncolinear if two) tracks. A fast tracking routine was then used and the following additional cuts were made.

(i) The distance of closest approach (DOCA) in the radial direction of both tracks in two-charged-prong events is required to be less than 2 cm. The Z position of the point of closest approach is required to be less than 10 cm from the interaction point. The track fit used did not include the primary vertex as part of the fit. For the four- or more-charged-prong events no DOCA cut was made.

(ii) The charges of tracks in two-prong events must be opposite.

The full tracking program was then used to reconstruct the event and log it to tape (KEEPASS2). Data summary tapes of interesting events types were made to further reduce the number of event types used for analysis.

B. General selection criteria

In reconstructing resonances produced in two-photon interactions a common set of initial cuts on charged and neutral tracks is used.

(1) The event must contain an even number of tracks with net charge zero.

(2) The tracking program must be able to find a vertex constrained fit to all charged tracks, with the vertex in the specified interaction region. All charged-track momenta are corrected for energy loss in the material preceeding the drift and vertex chambers.

(3) The charged tracks must hit the liquid-argon

calorimeter and time-of-flight counters within a fiducial region ($|Z| < 1.9$ meters). This ensures that for both real events and Monte Carlo events, most of the tracks satisfy the trigger requirements.

(4) To reduce annihilation background, we require that the total energy of all charged tracks seen be less than 40% of the total available energy. In a two-photon interaction most of the energy is carried away, unseen, by the outgoing beam electrons.

(5) Fake gammas are sometimes reconstructed near the position of a charged track's entry into a calorimeter. This is due mainly to energy deposited at some distance (which varies with the decay studied) from the path of the charged track by interactions in the magnet coil or calorimeter. To ensure that such gammas are not counted, all gammas within a given radius of a charged track are ignored.

(6) The detected gamma energy must be greater than 150 MeV for the liquid-argon (LA) and 200 MeV for the end caps to reduce fake gammas due to electronic noise. We also require that the tracking program not share more than 50% of the gamma's energy with any other gammas in the same module.

(7) The eight liquid-argon modules are separated from each other by dead regions where the efficiency for finding electromagnetic showers is low. We make a cut that avoids using gammas in these "cracks" between modules by requiring that $|\Delta\phi| > 0.9°$ from the crack centers.

(8) We require that no scattered beam electrons are detected by the small-angle tagger (SAT). This and cuts on the net p_t limit the Q^2 of the interacting virtual photons to small values.

C. Monte Carlo event simulation

To measure the acceptance, events were generated with the Monte Carlo program GGDEPA, which is based on a double-equivalent-photon approximation,[13] modified to actually reproduce the correct $|\sum \mathbf{P}_t|$ distribution and is, taken together with the subsequent detailed detector response simulation, a good measure of the acceptance. Electromagnetic showers were simulated with the full EGS code.

The two $\eta' \to \eta\pi^+\pi^-$ decays, reactions (2) and (3), have a spin-parity sequence of $J^P = 0^- \to 0^-0^-0^-$ so only a phase-space weighting is assumed for their generation. For the two decay modes $\eta' \to \rho\gamma$ and $a_2 \to \rho\pi$ the spin parity must be taken into account when the Monte Carlo events are generated, in order that the correct angular distribution of final-state particles be produced.

For the $\eta' \to \rho\gamma$ decay mode, reaction (1), the spin parities of $0^- \to 1^-1^-$ imply an $M1$ magnetic dipole transition for which the matrix element is[14]

$$|M|^2 \sim q_{\pi^+}^2 k_\gamma^2 M_{\pi^+\pi^-}^2 \sin^2\theta_{\text{helicity}} , \tag{2.1}$$

where q_{π^+} is the momentum of the π^+ in the $\pi^+\pi^-$ center-of-mass frame, k_γ the momentum of the γ in the $\pi^+\pi^-$ center-of-mass frame, $M_{\pi^+\pi^-}$ the invariant mass of the $\pi^+\pi^-$ system, and θ_{helicity} the helicity angle, defined as the angle between the three-momenta of the π^+ and γ in the $\pi^+\pi^-$ center-of-mass frame.

The weight to phase space due to the $\rho^0 \to \pi^+\pi^-$ resonance is

$$(\rho^0\text{-decay phase-space weight}) = \frac{M_{\pi^+\pi^-}}{q_{\pi^+}} \frac{\Gamma(M_{\pi^+\pi^-})}{(M_\rho^2 - M_{\pi^+\pi^-}^2)^2 + M_\rho^2 \Gamma^2(M_{\pi^+\pi^-})} ; \tag{2.2}$$

the decay width of the ρ^0 resonance is parametrized as

$$\Gamma(M_{\pi^+\pi^-}) = \Gamma(M_\rho) \frac{2q_{\pi^+}^3}{q_\rho(q_\rho^2 + q_{\pi^+}^2)} , \tag{2.3}$$

where M_ρ is the nominal ρ^0 mass, $\Gamma(M_\rho)$ the nominal width of the ρ^0, and q_ρ the momentum in the $\pi^+\pi^-$ center of mass at the nominal ρ^0 mass.

The $a_2 \to \rho\pi$ decay mode, when one photon is undetected, is a background to the decay mode $\eta' \to \rho\gamma$. The $a_2(1320)$, being a spin-2 particle, can be produced in two-photon interactions with total helicity 2 or 0. The Monte Carlo program used here assumes that the helicity 2 production mode dominates.

The matrix element for production of $a_2(1320)$ with helicity 2 is proportional to

$$\begin{aligned} |M|^2 \sim \Bigg| & P_{\rho^+}^2 P_{\pi^0} \sin\theta_{\rho^+} \sin\theta_{\pi^0} (\cos^2\theta_\rho \sin^2\phi_{\pi^0} + \cos^2\phi_{\pi^0})^{1/2} \left[\frac{M_{\pi^+\pi^0}}{P_{\pi^+}} \right]^{1/2} \frac{\sqrt{\Gamma(M_{\pi^+\pi^0})}}{(M_\rho^2 - M_{\pi^+\pi^0}^2) - iM_\rho\Gamma(M_{\pi^+\pi^0})} \\ & + P_{\rho^-}^2 P_{\pi^0} \sin\theta_{\rho^-} \sin\theta_{\pi^0} (\cos^2\theta_{\rho^-} \sin^2\phi_{\pi^0} + \cos^2\phi_{\pi^0})^{1/2} \left[\frac{M_{\pi^-\pi^0}}{P_{\pi^-}} \right]^{1/2} \frac{\sqrt{\Gamma(M_{\pi^-\pi^0})}}{(M_\rho^2 - M_{\pi^-\pi^0}^2) - iM_\rho\Gamma(M_{\pi^-\pi^0})} \Bigg|^2 . \end{aligned} \tag{2.4}$$

The decay width for the $\rho^\pm$ decay is given by

$$\Gamma(M_{\pi^\pm\pi^0}) = \Gamma(M_\rho) \frac{2P_{\pi^\pm}^3}{P_\rho(P_\rho^2 + P_{\pi^\pm}^2)} , \tag{2.5}$$

where $P_{\rho^\pm}$ is the momentum of the $\rho^\pm$ in the $\gamma\gamma$ center-of-mass frame, P_{π^0} the π^0 momentum in the $\pi^0\pi^\pm$ center-of-mass frame, $P_{\pi^\pm}$ the momentum of the $\pi^\pm$ in the $\pi^0\pi^\pm$ center-of-mass frame, $\theta_{\rho^\pm}$ the angle that the $\rho^\pm$ momentum makes with the $\gamma\gamma$ axis of collision in the $\gamma\gamma$ center-of-mass frame, θ_{π^0} the angle between the π^0

momentum in the ρ center-of-mass frame and the direction of the ρ in the $\gamma\gamma$ center-of-mass frame, and ϕ_{π^0} the azimuthal angle measured with respect to the plane defined by the $\gamma\gamma$ collision axis and the direction of the ρ, where the z axis is the direction of flight of the ρ.

It is important to note that for the above angles to be well defined, Lorentz boosts of the coordinate system must be done in the order: lab frame to $\gamma\gamma$ center of mass along the $\gamma\gamma$ collision axis in the lab frame, followed by $\gamma\gamma$ center of mass to the ρ center of mass along the ρ direction in the $\gamma\gamma$ center-of-mass frame.

Equation (2.4) contains the amplitude for the ρ resonance to be formed by either a $\pi^+\pi^0$ pair or a $\pi^-\pi^0$ pair. Since the final state is $\pi^+\pi^-\pi^0$, the intermediate ρ resonance is not directly observed, so that there is interference between the amplitudes for the ρ^+ and ρ^- intermediate states. All the final-state particles are bosons so a constructive interference is assumed. Such an interference is observed in the $a_2^{\pm} \to \rho^0\pi^{\pm}$ decay, where the ρ^0 can be explicitly reconstructed.

Equation (2.4) also includes the weight to phase-space terms[15] that take account of the ρ decay. Thus Eq. (2.4) includes the weighting factors used to weight the three-body phase-space distribution generated by the Monte Carlo program. The weighting of three-body phase space for the $\eta' \to \rho\gamma$ decay mode may be done separately [Eq. (2.2)] since no interference between intermediate states is present. This makes Eq. (2.4) slightly different from the usual definition of a matrix element of a decay, but this is necessary for practical programming reasons.

III. EVENT RECONSTRUCTION OF $\eta' \to \rho\gamma$ AND $a_2 \to \rho\pi$ DECAYS

A. Reconstruction of $\eta' \to \rho\gamma$

Events are discarded if more than one bona fide gamma is found in the event or if the distance between the gamma and a charged track is less than 35 cm. To help in reducing background from $\gamma\gamma \to e^+e^-\gamma$ several cuts are made. First we discard events whose charged tracks deposit more than 600 MeV in the liquid argon or whose momenta are greater than 2.0 GeV/c. This results in little loss of efficiency and further reduces the high-energy radiative electron background. Figure 3 shows the measured β vs momentum from TOF measurements on the charged tracks. A straight-line cut is made to remove the low-momentum high-β region populated by a large electron background. Below 150 MeV/c a significant fraction of the remaining background is found to be muons from QED events and pion decays.

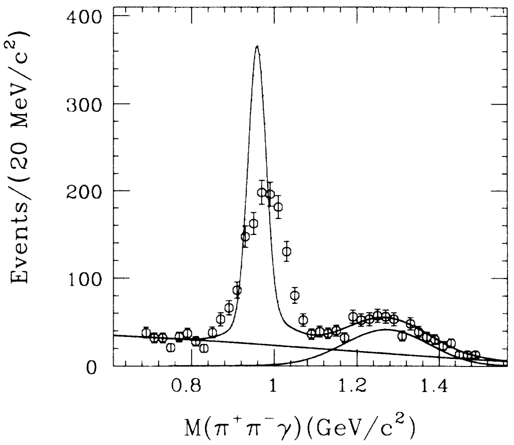

FIG. 4. The $\pi^+\pi^-\gamma$ mass distribution using the uncorrected γ energy. The fit to the data after gamma energy correction is superposed. Fits to the overall background (straight line) and the $a2(1320)$ contribution to the background are also shown.

The $\pi^+\pi^-\gamma$ mass using the measured gamma energy is shown in Fig. 4. The gamma direction is well measured while the gamma energy is not. This results in a broad η' peak somewhat displaced from the correct mass value. To improve the poor energy resolution of the observed gamma in $\eta' \to \rho\gamma$ events we take advantage of the kinematics of $\gamma\gamma$ interactions. For events with no tagging electron the net transverse momentum of produced η''s is

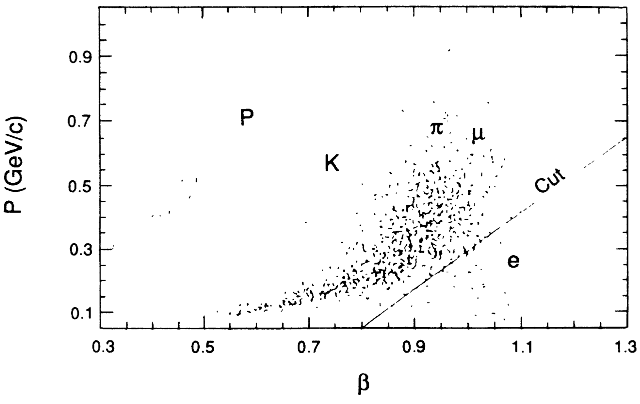

FIG. 3. Track beta vs momentum for four-prong events.

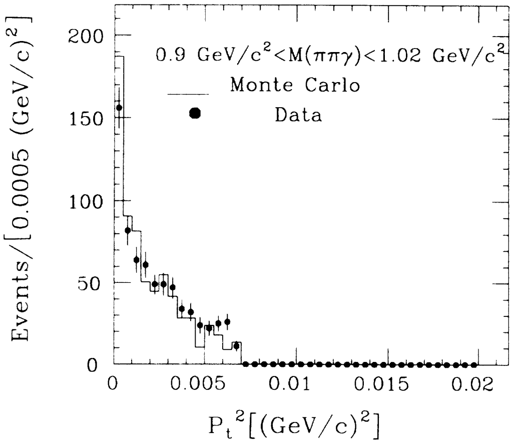

FIG. 5. The net P_t for Monte Carlo and real events, after energy correction.

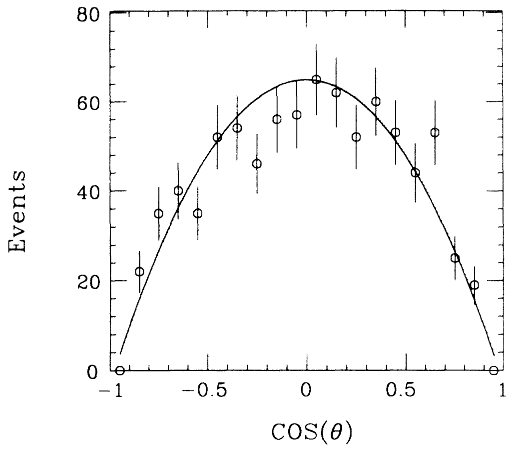

FIG. 6. Cosine of the helicity angle for events in the η' mass peak, background subtracted.

sharply peaked at zero. Thus we can adjust the gamma energy to balance the transverse momentum of the well measured π^+ and π^- while keeping the measured γ direction fixed.

A cut of 100 MeV/*c* on the net transverse momentum of the $\gamma\pi^+\pi^-$ system using the uncorrected gamma energy removes events for which not all of the decay products were seen. Events with a corrected gamma energy less than 150 MeV are also removed, to ensure that the corrected energy is consistent with the threshold energy for detecting the gamma.

The good agreement between the Monte Carlo simulation and the real event $|\sum \mathbf{P}_t|$ distribution in Fig. 5 indicates that background events with extra undetected neutrals are not a significant problem for events in the η' mass peak region.

Since the gamma energy correction method only requires that the magnitudes of the P_t of the $\pi^+\pi^-$ and gamma system be set equal and not their directions, it is still possible for the corrected $|\sum \mathbf{P}_t|$ to be nonzero. The $|\sum \mathbf{P}_t|$ of the $\gamma\pi^+\pi^-$ system using the corrected gamma energy is thus required to be less than 100 MeV/*c*, ensuring that corrected gamma momentum and transverse $\pi^+\pi^-$ momentum are reasonably opposite in direction.

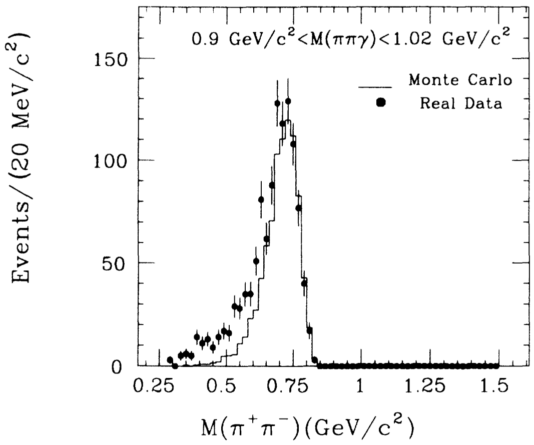

FIG. 8. The $\pi^+\pi^-$ mass for events in the η' peak.

Events of the form $ee \rightarrow eeee$ may look like $\pi^+\pi^-\gamma$ events when one of the electrons undergoes a hard bremsstrahlung. The gamma in this type of event tends to be radiated along the direction of one of the outgoing charged particles in the rest frame of the two charged particles. The helicity angle θ_{helicity} is defined as the angle that the gamma momentum three-vector makes with the π^+ three-momentum in the $\pi^+\pi^-$ center-of-mass frame. The forward peaking of helicity angle of the radiative background leads us to require that $|\cos\theta_{\text{helicity}}|$ be less than 0.8. Since the spin-parity of the η' decay leads to an amplitude proportional to $\sin^2\theta$, the radiative background is strongest where the desired signal is weakest. The background-subtracted helicity-angle distribution is shown in Fig. 6.

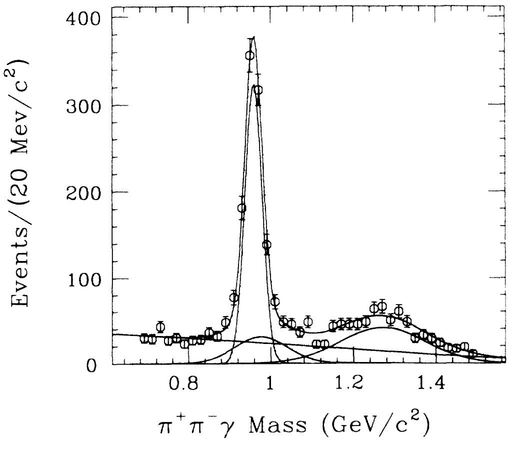

FIG. 7. The $\pi^+\pi^-\gamma$ mass after cuts. The overall fit is shown together with the background, $a_2(1320)$, and η' components.

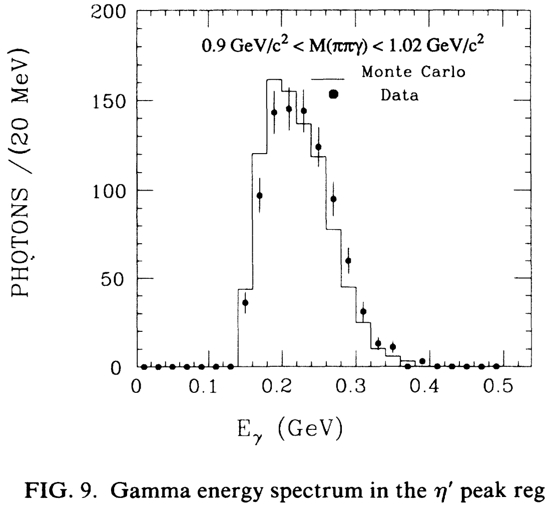

FIG. 9. Gamma energy spectrum in the η' peak region.

The spectrum resulting from the above cuts is shown in Fig. 7 and shows a narrower η' signal at the correct mass. We thus define the η' region between 0.90 and 1.02 MeV for the checks in Figs. 5, 6, 8, and 9. The fit to the $\pi^+\pi^-\gamma$ mass was done using a sum of four fitting functions. The $a_2(1320)$ background peak (described below) was fit with a single Gaussian whose mean and width were set by a fit to Monte Carlo–simulated events. it was found that for the η' a single Gaussian could not give a fit to the Monte Carlo–simulated data with a reasonable confidence level, so the η' peak was fit with two Gaussians, whose width and mean also were fixed by the Monte Carlo data. The fitting program constrained the ratio of the heights of the two Gaussians used in the η' fit to be fixed by Monte Carlo–simulated data. The remaining background was fit by a fourth-degree polynomial. The resulting fit to the real events gave a confidence level of about 15%.

The $\pi^+\pi^-$ mass for events in the η' peak region is shown in Fig. 8 and shows a clear ρ peak. A small excess of events over the Monte Carlo–simulation prediction can be attributed to events in the background under the η' peak in Fig. 7.

B. The reconstruction of $a_2 \rightarrow \rho\pi$ as a background

The process $\gamma\gamma \rightarrow a_2(1320) \rightarrow \rho^\pm\pi^\mp$; $\rho^\pm \rightarrow \pi^\pm\pi^0$; $\pi^0 \rightarrow \gamma\gamma$ when one of the gammas is not seen by the detector gives the observed final state of $\pi^+\pi^-\gamma$ and so appears as a background when looking at the decay mode $\eta' \rightarrow \rho^0\gamma$; $\rho^0 \rightarrow \pi^+\pi^-$.

The $a_2(1320)$ can be seen in Figs. 4 and 7 as a broad peak above the background. The Gaussian fit to the $a_2(1320)$ is centered at about 1270 MeV/c^2, considerably lower than the accepted mass of the $a_2(1320)$ of 1318 MeV/c^2 due to the missing gamma in the total invariant-mass calculation. The Monte Carlo simulation of $a_2 \rightarrow \rho\pi$ correctly predicts the observed $\pi^+\pi^-\gamma$ mass distribution.

If one looks at the $\pi^+\pi^-$ mass of events in the $\pi^+\pi^-\gamma$ mass region of the $a_2(1320)$ (between 1200 MeV/c^2 and 1450 MeV/c^2) there is a broad but distinct peak at about 950 MeV/c^2. The $a_2(1320)$ Monte Carlo calculation does not predict such a peak. In fact the peak is due to the background of low-energy gammas. Since there are more background gammas as the gamma energy decreases, $\pi^+\pi^-\gamma$ masses in the $a_2(1320)$ region coming from background events are more likely to be formed by a low-energy background gamma and a pair of charged particles whose $\pi^+\pi^-$ invariant mass is large. The fit to signal and background for the $\pi^+\pi^-$ mass was in fact consistent with the fit to the signal and background in the $a_2(1320)$ region of the $\pi^+\pi^-\gamma$ mass.

The $\pi_2(1680)$ has recently been seen in two-photon collisions.[16,17] In addition to the background from the $a_2(1320)$, the decay of the $\pi_2(1680)$ is a potential background to $\pi^+\pi^-\gamma$ when it decays by $\pi_2(1680) \rightarrow f^0\pi^0$; $f^0 \rightarrow \pi^+\pi^-$. Monte Carlo simulations show that the π_2 (1680) contributes only to the high-mass background.

C. Systematic errors

Systematic errors from all sources are separately discussed and summarized in Table III for each decay mode.

1. Systematic error in e^+e^- luminosity measurement

The e^+e^- luminosity is measured in the Mark II detector by observing Bhabha scattering of the electrons and positrons with the SAT. The systematic error in the luminosity is almost totally due to the systematic error in the knowledge of the efficiency of the luminosity monitor and has been estimated at about 5%,[18] based on a comparison with wide-angle Bhabha-scattering events.

2. Systematic error in drift-chamber tracking-efficiency corrections

The drift-chamber efficiency for finding single tracks changed considerably during the part of the PEP running from which our data are taken. Corrections for drift-chamber efficiency have been measured in connection with other data analyses,[19] and were found to be independent of track momentum, angle, and track multiplicity. The correction is estimated to introduce no more than about 3% systematic error to the two-photon width measurements.

3. Systematic error in the background subtraction

The number of events found in the η' and $a_2(1320)$ peaks for the $\pi^+\pi^-\gamma$ mass distribution depends somewhat on the fitting method. When a fit parameter is fixed it is set equal to the value found in a fit to the Monte Carlo events. Three such methods of fitting the η' peak with Gaussians were tried: (a) Fix the ratio of heights, center positions, sigmas; (b) fix the ratio of heights only; (c) fix the center positions only. For the η' peak the largest variation with fitting method is 2.7%. The height of the Gaussin fitting the $a_2(1320)$ peak is effected by the fits to the background and the η' peak. The largest variation with fitting method for the $a_2(1320)$ peak is 17%.

4. Systematic error due to Monte Carlo simulation

For the $\eta' \rightarrow \rho\gamma$ decay mode the simulation of the liquid-argon calorimeter efficiency contributes the most important systematic error, due to the low energies of the gammas. About 36% of the gammas in the signal events have energies below 200 MeV (see Fig. 9). In this energy range the detection efficiency is changing rapidly, so to make the simulation of gammas as accurate as possible Monte Carlo events were generated using the full EGS electromagnetic-shower program.

The Monte Carlo simulation's efficiency was compared to beam-test data, and they agree within statistical errors for gamma energies greater than 200 MeV. Comparison of efficiencies below 200 MeV suggest a systematic error of 10% in the efficiency due to Monte Carlo simulation of the liquid-argon calorimeter. The uncertainty in the end-cap efficiency contributes less than 0.2% to the systematic error in the two-photon width.

TABLE I. Recent measurements of $\Gamma_{\eta'\to\gamma\gamma}$.

Experiment	$\Gamma_{\eta'\to\gamma\gamma}$ (keV)	Mode	Reference
Mark II (SPEAR)	$5.8\pm1.1\pm1.2$	$\rho\gamma$	1
JADE	$5.0\pm0.5\pm0.9$	$\rho\gamma$	2
CELLO	$5.4\pm1.0\pm0.7$	$\rho\gamma$	3
PLUTO	$3.80\pm0.26\pm0.43$	$\rho\gamma$	4
TASSO	$5.1\pm0.4\pm0.7$	$\rho\gamma$	5
JADE	4.0 ± 0.9	$\gamma\gamma$	6
Crystal Ball	$5.0\pm0.6\pm0.8$	$\gamma\gamma$	7
TPC/2γ	$4.5\pm0.3\pm0.7$	$\rho\gamma$	8
ARGUS	$3.76\pm0.13\pm0.47$	$\rho\gamma$	9
Crystal Ball	$4.6\pm0.4\pm0.6$	$\eta\pi^0\pi^0$	10
Mark II (PEP)	$4.61\pm0.32\pm0.57$	$\rho\gamma$	This paper
Mark II (PEP)	$4.37\pm0.62+0.96-0.94$	$\eta\pi^+\pi^-$	This paper
Mark II (PEP)	$4.60\pm0.49+0.65-0.95$	$\pi^+\pi^-\pi^+\pi^-$	This paper

D. Trigger-efficiency corrections

A detailed discussion of the trigger-efficiency measurement is given in Appendix A. This trigger efficiency correction for the $\eta'\to\rho\gamma$ decay mode is about 8%. The systematic error introduced is estimated at 3.3% of the $\gamma\gamma$ rate.

E. Results

The measured luminosity and efficiency are used to convert the number of events observed to a cross section

$$\sigma(e^+e^-\to e^+e^-R)=\frac{N_{R_{\text{observed}}}}{\epsilon_R\int L\,dt}\ .$$

The effective efficiency is given by

$$\epsilon_R=\epsilon_{\text{track}}\epsilon_{\text{MC}}(\epsilon_1 W_1+W_2)\ ,$$

where ϵ_{MC} is the raw Monte Carlo–simulation efficiency; ϵ_{track} reflects the variation in drift-chamber tracking efficiencies over the course of the experiment; ϵ_1 is the KEEPASS2 recovery efficiency; W_1 is the KEEPASS2 data-set weight; and W_2 is the normal PASS2 data-set weight, with $W_1+W_2=1$. The effective luminosity $\int L\,dt=C(W_1L_1+W_2L_2)$ and is the corrected weighted sum of the KEEPASS2 and PASS2 luminosities used. Table IV shows the effective efficiencies and luminosities for the several resonance decays studied.

The relation between the measured cross section and the radiative width can be expressed by a modified Low formula:

$$\sigma(e^+e^-\to e^+e^-R)=\frac{16\alpha^2}{M_R^3}\ln\left[\frac{E_b}{m_3}\right]^2 \times f\left[\frac{M_R}{2E_b}\right](2J+1) \times(\text{field correction})\ ,$$

where

$$f(x)=(2+x^2)^2\ln\left[\frac{1}{x}\right]-(1-x^2)(3+x^2)\ .$$

The Field correction[20] takes into account the correlations between the virtual gammas in calculating the effective $\gamma\gamma$ luminosity and is given as the ratio of the true luminosity to that obtained in the leading-log approximation. The leading-log approximation in turn differs from the Low formula by a factor $\ln(2E_{\text{beam}}/m_e)/\ln(E_{\text{beam}}/m_e)$.[21] The net Field correction is then 0.88 at the η' mass. Hence,

$$\Gamma(\eta'\to\gamma\gamma)(\text{in keV})=2.676\sigma(e^+e^-\to e^+e^-\eta')\ (\text{in nb})$$

and

TABLE II. Recent measurements of $\Gamma_{a_2(1320)\to\gamma\gamma}$.

Experiment	$\Gamma_{a_2(1320)\to\gamma\gamma}$ (keV)	Reference
Crystal Ball (SPEAR)	$0.77\pm0.19\pm0.27$	25
CELLO	$0.81\pm0.19\pm0.27$	26
JADE	$0.84\pm0.07\pm0.15$	27
PLUTO	$1.06\pm0.18\pm0.19$	28
Crystal Ball (DORIS)	$1.14\pm0.20\pm0.26$	29
TASSO	$0.90\pm0.27\pm0.16$	30
TPC/2γ	$0.90\pm0.09\pm0.22$	31
Mark II	$1.03\pm0.13\pm0.21$	This paper

TABLE III. A summary of errors affecting $\Gamma_{\gamma\gamma}$ measurements.

Decay mode	$\eta' \to \rho\gamma$	$a_2 \to \rho\pi$	$\eta' \to \eta\pi^+\pi^-$ $\eta \to \gamma\gamma$	$\eta' \to \eta\pi^+\pi^-$ $\eta \to \pi^+\pi^-\pi^0$ $\eta \to \pi^+\pi^-\gamma$
Luminosity measurement	±5%	±5%	±5%	±5%
Tracking efficiency	±3%	±3%	±3%	−15%
Background subtraction	±2.7	±17%	±3.2%	±1%
MC simulation of γ's	±10%	±10%	±20%	
Hand scan			+5% −2%	
Trigger efficiency	±3.3%	±3.3%	±4%	±11.4%
Vertex cut				±6.8%
Total	±12.3%	±20.8%	22.0%	+14.2%
Systematic error			−21.5%	−20.7%
$\Gamma_{\gamma\gamma}$ (keV)	4.61	1.03	4.37	4.60
Statistical error	±0.32	±0.13	±0.62	±0.49
Systematic error	±0.57	±0.21	+0.96 −0.94	+0.65 −0.95

$$\Gamma(a_2 \to \gamma\gamma) = 1.579\sigma(e^+e^- \to e^+e^-a_2) .$$

The corrected decay widths measured in this section are then

$$\Gamma_{\eta' \to \gamma\gamma} = 4.61 \pm 0.32 \pm 0.57 \text{ keV} ,$$

$$\Gamma_{a_2 \to \gamma\gamma} = 1.03 \pm 0.13 \pm 0.21 \text{ keV} ,$$

where the first error is statistical and the second systematic. These widths are summarized in Tables I and II. The systematic errors are summarized in Table III.

IV. THE DECAY $\eta' \to \eta\pi^+\pi^-$; $\eta \to \gamma\gamma$

This section describes the reconstruction of two-photon events with the final observed particles $\pi^+\pi^-\gamma\gamma$.

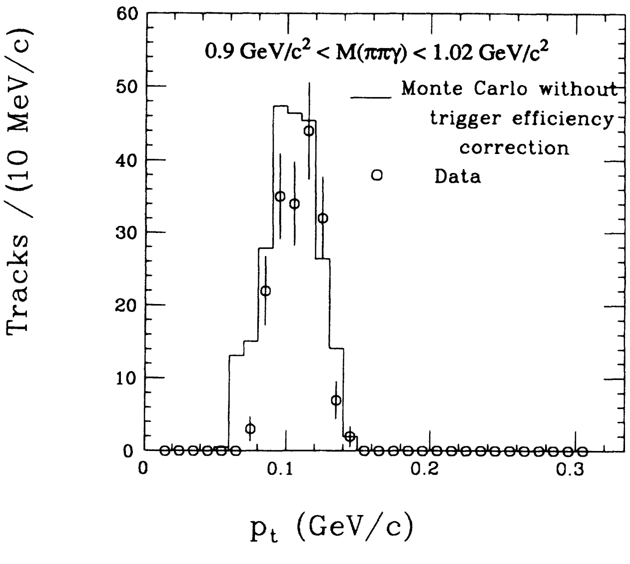

FIG. 10. Smallest P_t of the two pions in the η' peak.

A. Additional selection criteria

Figure 10 shows the transverse momentum of the smaller-momentum track for events in the η' peak region, uncorrected for trigger efficiency. The agreement with the Monte Carlo data is quite good when the P_t of each charged track is required to be at least 90 MeV/c. The trigger efficiency correction is very important here since the decay $\eta' \to \eta\pi^+\pi^-$ has only a small Q value (129 MeV). This trigger correction (see Appendix) to the Monte Carlo–calculated efficiency for this decay mode is 33% and is the largest trigger correction for the decay modes considered in this paper.

To further reduce electron, kaon, and proton backgrounds TOF cuts are made on the charged tracks.

B. Reconstruction of the η for $\eta \to \gamma\gamma$

Figure 11 shows the raw $\gamma\gamma$ invariant mass. We see that the $\gamma\gamma$ mass for Monte Carlo–simulated events is

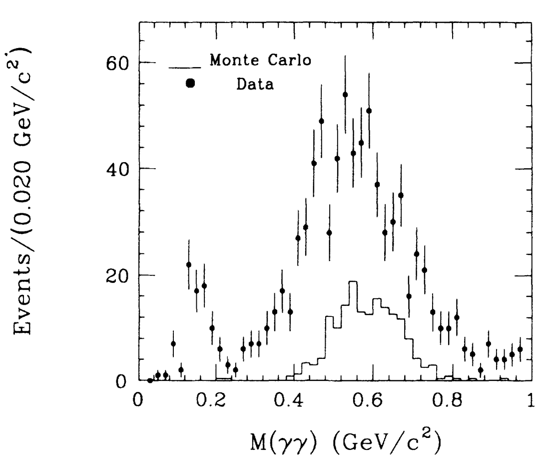

FIG. 11. $\gamma\gamma$ mass before the η mass constraint. Histogram shows the expected signal from η' decays.

very broadly distributed around the η mass. The normalization was chosen to represent the number of η's coming from our η' signal events. Most of the real events in Fig. 11 above a $\gamma\gamma$ mass of 250 MeV/c^2 come from a combinatorial background whose peak shifts as the energy of the lowest-energy gamma accepted is changed.

If the gamma energies measured by the liquid-argon calorimeter were used together with the measured pion momenta to find the $\pi^+\pi^-\gamma\gamma$ invariant mass, the mass resolution would be dominated by the relatively poor gamma energy measurement. To overcome this we make use of the good position resolution of the calorimeters and adjust the measured gamma energies assuming that the gammas we are considering come from an $\eta\rightarrow\gamma\gamma$ decay. The fit has one constraint and is easily done analytically.

All gammas that pass the initial cuts are paired for consideration in the fit to the η. The following additional cuts are then made.

(1) Reject events with end-cap gammas because of the poor energy resolution and uncertain efficiency of the end caps.

(2) Require that the gammas have an energy greater than 200 MeV.

(3) The χ^2 of the fit to the $\eta\rightarrow\gamma\gamma$ hypothesis must be less than 5.0. This corresponds to a fit confidence level of at least 2.5%.

(4) Both gammas in the pair must be at least 20 cm away from the nearest charged track in the liquid-argon calorimeter to reduce fakes.

(5) No extra gammas may be present in the event. The selection criteria for extra gammas are described below.

(6) The invariant mass of the two photons in the pair must be greater than 450 MeV/c^2 and less than 750 MeV/c^2. This cut, determined from the Monte Carlo simulation, ensures that the measured gamma energies and directions are at least reasonably consistent with the hypothesis that they are from an η decay.

(7) When the fit η momentum is added to the momentum of the charged tracks, the $|\sum \mathbf{P}_t|$ of the $\eta\pi\pi$ system is then required to be less than 200 MeV/c. This reduces background events from "feed down" where not all the final-state particles were seen.

After two gammas are selected as a trial pair for a fit to the decay $\eta\rightarrow\gamma\gamma$ the remaining gammas are evaluated as to whether they count as "extras," with any one of the following criteria.

(1) A gamma is extra if its energy is greater than 150 MeV and is isolated in its own module, not sharing the same liquid-argon module with another gamma or charged track.

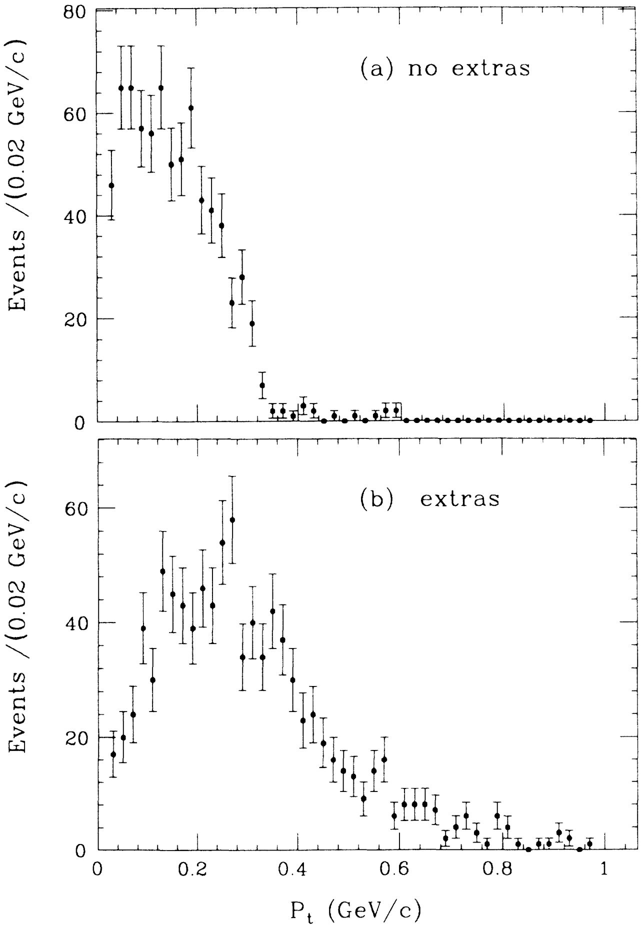

FIG. 12. $\sum P_t$ of $\eta\pi^+\pi^-$ system for events with (a) no "extra" gammas, and (b) "extra" gammas.

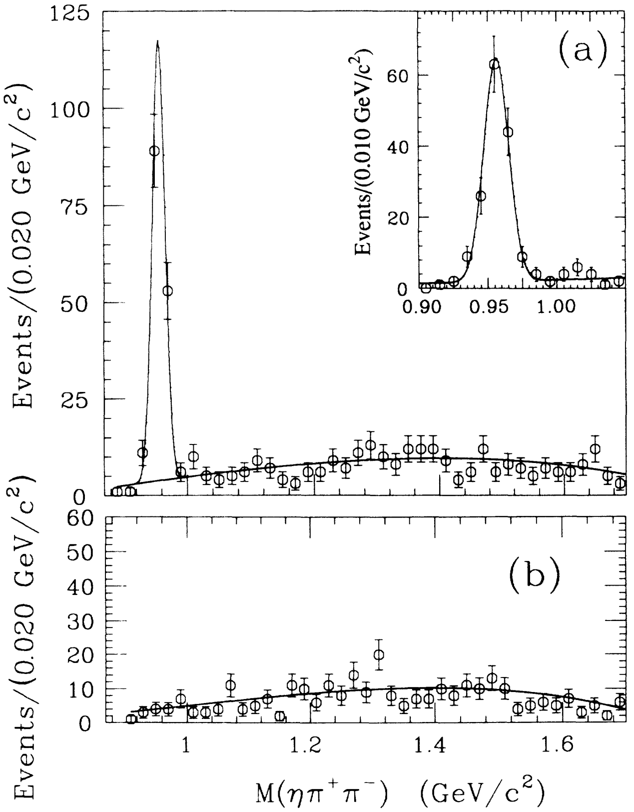

FIG. 13. The $\eta\pi^+\pi^-$ mass for events with (a) no "extra" gammas, and (b) "extra" gammas.

(2) A gamma is extra if it is at least 20 cm away from any other gamma or charged track and has an energy greater than 200 MeV.

(3) A gamma is extra if it is at least 20 cm away from any other gamma or charged track and has an energy greater than 150 MeV and the tracking program indicates that it shares no more than 5% of its energy with any other electromagnetic shower in the liquid-argon calorimeter.

As a check of the effectiveness of the above cuts for extra gammas we can look at the $|\sum \mathbf{P}_t|$ of the reconstructed $\eta\pi^+\pi^-$ system, with and without extra gammas found. Figure 12 shows a broader $|\sum \mathbf{P}_t|$ distribution for events with extra gammas indicating that not all final-state particles are accounted for. We may also look at the final $\eta\pi^+\pi^-$ mass distribution with and without an extra gamma found. In Fig. 13, the events with no extra gammas show a clear η' peak, but there is no η' peak for events with extra gammas.

C. Backgrounds for $\eta' \to \eta\pi^+\pi^-$, $\eta \to \gamma\gamma$ events

The background from annihilation events is further reduced to less than 0.4% by a cut on the total energy seen after the fit.

Internal and external bremsstrahlung production of final-state gammas is much less of a problem here than for $\eta' \to \rho\gamma$ since two final-state gammas must be produced. Any remaining radiative background has no mass peak structure and so will be automatically subtracted.

The main difficulties in eliminating the background have to do with ensuring that we have two and only two real photons in the final state.

The extra gamma criterion eliminates most of the feed-down background but there are also backgrounds that require hand scanning. The types of events thus discarded were the following.

(1) Events with obvious untracked additional particles in the drift chamber, especially low-energy tracks, indicated by the presence of unassigned drift-chamber wire hits.

(2) Events with obvious cosmic-ray tracks. The most common case involves a high-energy cosmic track which crosses the drift chamber missing the interaction point leaving hits in the liquid argon as it enters and exits. Because the drift-chamber tracking program only looks for tracks that pass close to the interaction point the energy deposits in the liquid argon were classified as coming from two gammas.

(3) False gammas can be accepted when a track in the drift chamber has been poorly tracked. Since the path of the track is poorly known the projected entry point in the liquid-argon calorimeter may be far enough away from the actual entry position so that the shower found in the liquid argon due to the charged track is thought to be due to a photon. A look at the drift-chamber wire hits can indicate that the charged track has scattered or decayed.

(4) Events with obvious untracked gamma conversions ($\gamma \to e^+e^-$) are removed since there is then clearly an extra gamma in the event. Gamma conversions are easily identified by the near zero opening angle of the two charged tracks produced, usually at some distance from the interaction point.

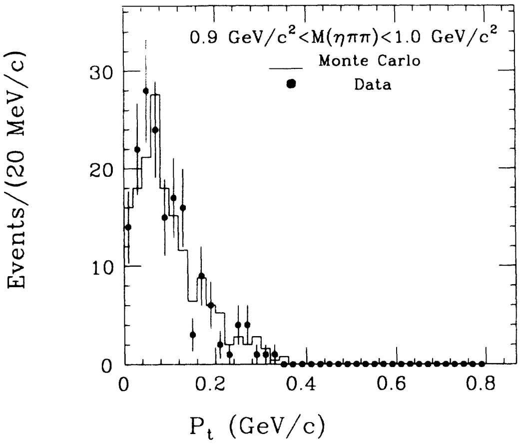

FIG. 14. Net transverse momentum of the $\eta\pi^+\pi^-$ system for events in the η' peak.

The hand scan rejects about 5% of the events in the η' peak mass region.

As an indication of the effectiveness of the cuts used to eliminate background events, we can look at the $|\sum \mathbf{P}_t|$ of events in the η' peak. (See Fig. 14.) The excellent agreement between the real data with the Monte Carlo simulation demonstrates that the residual background is not significant.

D. Systematic errors

The systematics errors due to the measurement of the e^+e^- luminosity and the corrections for trigger efficiency due to changes in drift-chamber tracking efficiency also apply to this decay mode. Additional sources of systematic error were.

1. Systematic errors due to hand-scanning candidate events

To understand the systematic error introduced by the unavoidable subjective judgments in hand-scanning events for background, two hand scans were done, several months apart. A conservative estimate of the hand-scan systematic error would be +5%, −2%.

2. Systematic error due to Monte Carlo simulation

Because of the low transverse momentum of the charged π's produced in this decay mode, we must also consider the systematic error due to the estimate of the trigger efficiency of low P_t tracks. The correction is about 33%, and the systematic error introduced is estimated at 4%.

The Monte Carlo–simulated efficiency is very sensitive to the correct modeling of the photon interactions in the calorimeters. Although EGS was used for all the Monte Carlo event simulation, we are conservative. A ±20%

systematic error due to shower simulation in the liquid argon seems in order for this decay mode.

To estimate the effect that an error in end-cap efficiency in the Monte Carlo simulation would have on the two-photon width, the analysis program was run on Monte Carlo–simulated events with and without the veto of events with end-cap gammas. No difference in number of events in the final η' peak was found. Vetoing events with end-cap gammas removes only the background, so the systematic error due to end-cap efficiency can be neglected.

3. *Systematic errors due to background subtraction*

The number of events found in the η' peak varies with fitting method. Three fit methods were tried: (1) all parameters free; (2) sigma fixed; (3) sigma fixed and center position fixed. The largest variation with fit method was $+3.2\%$. A conservative systematic error would be $\pm 3.2\%$. The systematic errors are again summarized in Table III.

E. Results

Using the combined efficiency given in Table IV and the procedure described in Sec. III E the radiative width[22] for this decay mode is then found to be

$$\Gamma_{\eta' \to \gamma\gamma} = 4.37 \pm 0.62 \pm 0.96 \text{ keV} .$$

V. THE DECAY $\eta' \to \eta\pi^+\pi^-$, $\eta \to \pi^+\pi^-\pi^0, \pi^+\pi^-\gamma$

This section describes the reconstruction of η' events with the final observed particles $\pi^+\pi^-\pi^+\pi^-$.

A. Selection criteria

The Mark II detector is exceptional in that its charged trigger is sensitive to charged tracks with transverse momenta as low as 90 MeV/c, and the drift chambers can actually track additional particles at much lower momenta. The decay mode we are considering produces tracks with P_t's that are almost all less than 200 MeV/c.

Because this decay mode of the η' has four charged particles in the final state, it is not subject to the same kinds of backgrounds considered earlier for the other η' decay modes. In adjusting the selection criteria we found that a good signal with relatively low background could be obtained by only requiring four charged tracks with net charge zero and visible energy less than 0.4 $E_{\text{c.m.}}$.

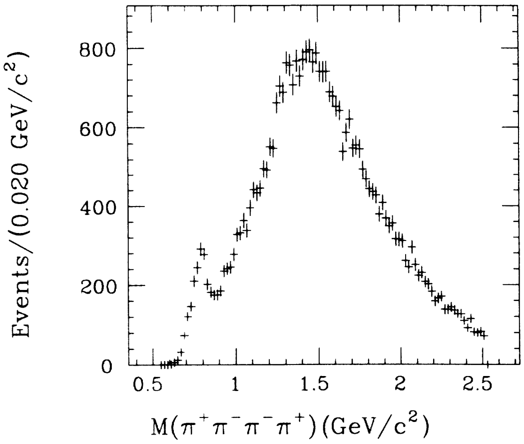

FIG. 15. Four-pion invariant mass for events passing "quality" cuts only.

A clear peak can be seen in the histogram of the resulting 4π invariant mass in Fig. 15. Because we do not include the contribution to the invariant mass of the π^0 or the γ from the decay of the η, the η' peak is shifted down in mass from 958 MeV/c^2 to about 800 MeV/c^2.

To further reduce the background we make the following additional cuts.

(1) We require that the position within the detector of the point on a track at the minimum distance of approach to the beam origin simply be near the interaction point. Its z position (distance along the beam axis) was required to be within 50 cm of the interaction point and its distance away from the beam axis to be within 5 cm. These cuts were so loose because of the relatively large multiple scattering and decay probability of the very-low-momentum charged pions.

(2) Because the desired final state has four charged particles, backgrounds due to QED, being higher order in α, are greatly reduced. Such four charged-particle final states can, however, be produced by radiative QED events with pair production or by non-QED sources such as $\eta' \to \rho\gamma$ with gamma conversion. To reduce such backgrounds with electrons in the final state, TOF and opening angle cuts were applied.

(3) Some final states involving kaons (such as $K^0K^+\pi^-; K^0 \to \pi^+\pi^-$ and $K^+K^-\pi^+\pi^-$) can produce a four final-state background. The K^0 background is re-

TABLE IV. A summary of effective efficiencies.

Decay mode	Effective efficiency	Effective luminosity (pb^{-1})
$a_2 \to \rho\pi$	0.609%±0.035%	181
$\eta' \to \rho\gamma$	1.024%±0.028%	177
$\eta' \to \eta\pi^+\pi^-$; $\eta \to \gamma\gamma$	0.249%±0.027%	171
$\eta' \to \eta\pi^+\pi^-$; $\eta \to \pi^+\pi^-\pi^0$, $\pi^+\pi^-\gamma$	1.152%±0.152%	175

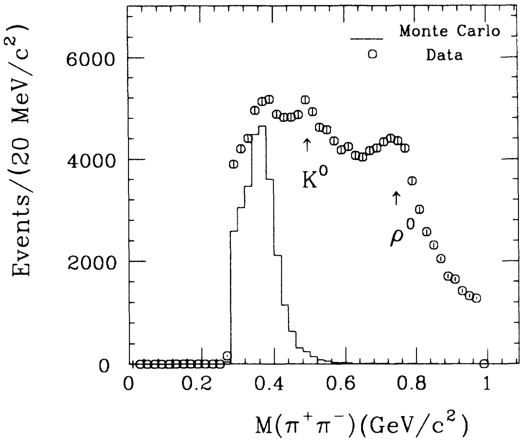

FIG. 16. The $\pi^+\pi^-$ mass for all oppositely charged-track combinations. The corresponding Monte Carlo prediction for the pions from η' decay is shown as the solid histogram.

duced by requiring that the invariant mass of all opposite charge combinations be in a range that excludes the K^0 mass of $450\ \mathrm{MeV}/c^2 < M_{\pi^+\pi^-} < 550\ \mathrm{MeV}/c^2$. The $\pi^+\pi^-$ mass spectrum in Fig. 16 shows a distinct peak at the K^0 from $K_{\mathrm{short}} \rightarrow \pi^+\pi^-$ as well as a broad shoulder near 770 MeV/c^2 caused by the dominant $\rho^0 \rightarrow \pi^+\pi^-$ decay. The low track momenta of events in the η' peak region make TOF cuts to remove $K^{\pm}$ very effective.

The 4π mass distribution after all the above cuts is shown in Fig. 17. The background is now substantially reduced. Figure 18 shows the $|\sum \mathbf{P}_t|$ of all four charged tracks for events in the peak. It is not peaked at zero because of missing neutral final-state particles and matches well with the Monte Carlo prediction.

B. Systematic errors

1. Systematic error due to Monte Carlo simulation

The detection of the decay mode $\eta' \rightarrow \eta\pi^+\pi^-$; $\eta \rightarrow \pi^+\pi^-\pi^0$, $\pi^+\pi^-\gamma$ relies only on finding the charged π's in these decays. We therefore avoid systematic errors introduced by trying to detect the gammas in the final state. The track-finding systematic error is confined to the detection efficiency and measurement errors of charged tracks.

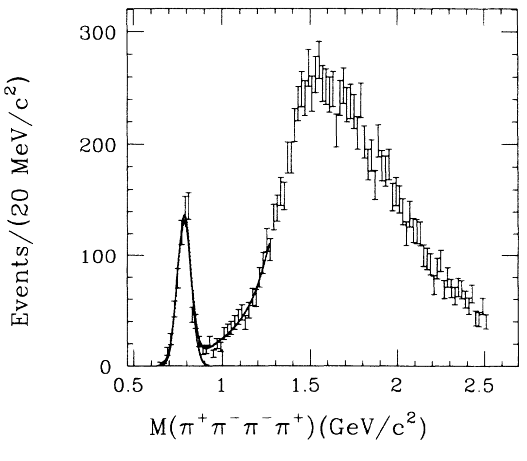

FIG. 17. Four-pion invariant mass after all cuts.

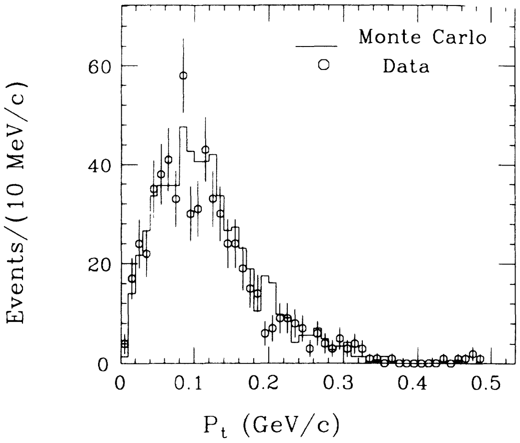

FIG. 18. Net transverse momentum of the four-pion system for events in the "η' mass" region.

The track position cut is a source of systematic error in our measurement of $\Gamma_{\eta' \rightarrow \gamma\gamma}$ if the Monte Carlo simulation does not have the same position distribution as the real events. To assess this systematic error the 4π mass distribution was fit with the track position cut removed and compared to the 4π mass distribution with the cut. Removing the track position cut increased the number of η' events found for Monte Carlo data by 36%. For real data the increase was 42%. This change alone increases $\Gamma_{\eta' \rightarrow \gamma\gamma}$ by about 4%. The background under the η' peak also increased but is subtracted by the fit.

Ideally we would like to eliminate the track position cut (42% more events), but the trigger efficiency is very sensitive to the vertex cuts made, and introduces an even larger systematic error into the $\Gamma_{\eta' \rightarrow \gamma\gamma}$ measurement than that introduced by the vertex cut iself. Using tight and loose vertex cuts we estimate that the systematic error due to the vertex cut is roughly 10%.

In addition to track fitting errors, we face the possibility that the efficiency for finding tracks may be different for Monte Carlo and real events. To check on this possibility we looked at the distribution of the angles that tracks make with the beam axis for events with 4π mass within the η' peak region. If we compare the Monte Carlo simulation to real data, we do see a small loss of efficiency at small angles, since these tracks pass through fewer drift-chamber layers. For the mass range we are interested in we loose about 4% more tracks in the real events than in the Monte Carlo simulation, implying about a +4% systematic error in $\Gamma_{\eta' \rightarrow \gamma\gamma}$. However, no $|\cos\theta|$ cut is done on the track momenta since the systematic error introduced is relatively small and such a cut would result in a significant loss of events.

The tracking efficiency correction for the four prongs is about twice as large as for the two-prong decay modes,

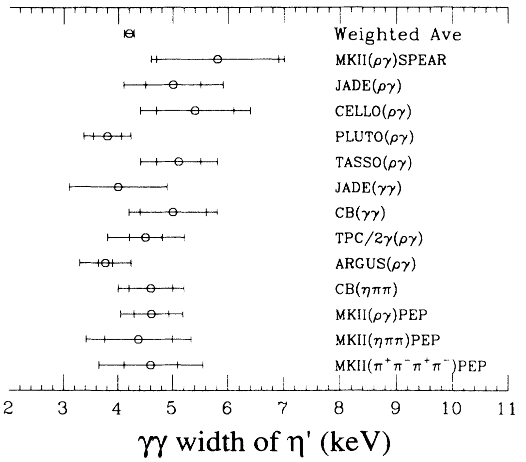

FIG. 19. Recent measurements of the η' two-photon width.

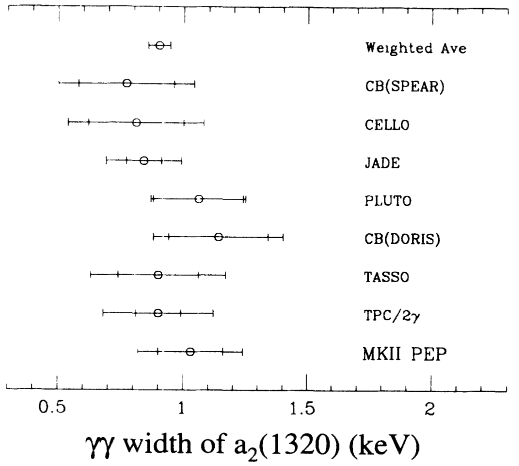

FIG. 20. Recent measurements of the $a2(1320)$ two-photon width.

so we must reassess its contribution to the systematic error. As a check, the $\Gamma_{\eta'\to\gamma\gamma}$ was calculated using only the "good" data, i.e., data taken during a period when there was no significant loss of drift-chamber tracking efficiency, and gave a two-photon width which is smaller by 23%. If we failed to correct for the tracking efficiency the two-photon width would change by only 15%. Therefore the largest systematic error that can be contributed to the tracking-efficiency correction is −15%.

2. *The trigger-efficiency correction*

The trigger-efficiency correction for the $\eta'\to\eta\pi^+\pi^-$; $\eta\to\pi^+\pi^-\pi^0$, $\pi^+\pi^-\gamma$ decay mode is about 25%. The systematic error introduced is estimated at 17%.

3. *Systematic errors due to background subtraction*

The number of events found in the η' peak varies with fitting method. Four fit methods were tried: (1) all parameters free; (2) sigma fixed; (3) sigma fixed and center position fixed; (4) center position fixed. The largest variation with fit method was +0.6%. A reasonable systematic error would be ±1%. The systematic errors are again summarized in Table III.

C. Results

Again using the effective efficiency in Table IV, the procedure of Sec. III E gives a measured decay width for this decay mode of

$$\Gamma_{\eta'\to\gamma\gamma}=4.60\pm0.49+0.65-0.95 \text{ keV} .$$

VI. CONCLUSIONS

The statistically weighted average of our three measurements is

$$\Gamma(\eta'\to\gamma\gamma)=4.57\pm0.25\pm0.44 \text{ keV} .$$

This can be compared to the previous world average width of 4.20±0.091 keV.[23] Using the Particle Data Group average[24] for the branching ratio of the $\eta'\to\gamma\gamma$ branching ratio of 0.0196±0.0015 together with our radiative width gives a total η' width $\Gamma=233\pm13\pm50$ keV.

Table I and Fig. 19 compare our η' two-photon width measurements to recent measurements. Similarly, Table II and Fig. 20 compare our $a_2(1320)$ two-photon width measurement to others. Note that the weighted averages given in both the above figures use the quoted statistical error only.

Table III summarizes the systematic errors in all of our width measurements.

Table IV summarizes the detector efficiencies for all the decay modes presented in this paper.

Since the SU(3)-flavor symmetry is broken by the large mass of the strange quark, the observable isoscalars η and η' are mixtures of the SU(3)-singlet (η_1) and -octet (η_8) basis states. The mixing is usually parametrized in terms of one angle Θ:

$$\begin{aligned}
\eta_1&=(d\bar{d}+u\bar{u}+s\bar{s})/\sqrt{3} ,\\
\eta_8&=(d\bar{d}+u\bar{u}-2s\bar{s})/\sqrt{6} ,\\
\eta(549)&=\cos\Theta\,\eta_8-\sin\Theta\,\eta_1 ,\\
\eta'(958)&=\sin\Theta\,\eta_8+\cos\Theta\,\eta_1 .
\end{aligned} \tag{6.1}$$

Neglecting any possible mass dependence, the ratios of the coupling constants within the SU(3) nonet then depend only on the quark charges and mixing angle:

$$g_{\pi^0_{\gamma\gamma}}:g_{\eta\gamma\gamma}:g_{\eta'_{\gamma\gamma}}=\langle e_q^e\rangle_{\pi^0}:\cos\Theta\langle e_q^2\rangle_8-\sin\Theta\langle e_q^2\rangle_1:\sin\Theta\langle e_q^2\rangle_8+\cos\Theta\langle e_q^2\rangle_1 , \tag{6.2}$$

where the two-photon coupling constants for the pseudoscalar mesons are related to their two-photon widths by

$$\Gamma_{M\to\gamma\gamma}=\frac{m_M^3}{16\pi}g_{M_{\gamma\gamma}}^2 \ . \tag{6.3}$$

The calculated two-photon width of the π^0 gives a value[32] (7.63 eV) that matches well with the experimental value (7.85±0.54 eV) when three color degrees of freedom are assumed for the constituent quarks.

If we assume SU(3)-flavor symmetry, then we can equate the pseudoscalar decay constants, $f_\pi=f_{\eta_s}=f_{\eta_1}$. The two-photon width of the π^0 can then be used to find the widths of the η and η' as a function of mixing angle Θ. This allows us to write Eq. (6.2) in the form

$$\frac{\Gamma_{\pi^0\to\gamma\gamma}}{m_{\pi^0}^3}:\frac{\Gamma_{\eta\to\gamma\gamma}}{m_\eta^3}:\frac{\Gamma_{\eta'\to\gamma\gamma}}{m_{\eta'}^3}=3:(\cos\Theta-\sin\Theta\, 2\sqrt{2})^2:(\sin\Theta+\cos\theta\, 2\sqrt{2})^2 \ . \tag{6.4}$$

Chanowitz, however, points out[33] that the assumption that $f_{\eta_8}=f_{\eta_1}$ may not be justified by SU(3)-flavor symmetry, since it is really equivalent to the assumption that the wave functions of flavor octet and singlet are the same.

More generally one can write[34]

$$\begin{aligned}\frac{\Gamma(\eta\to\gamma\gamma)}{\Gamma(\pi^0\to\gamma\gamma)}&=\left[\frac{m_\eta}{m_\pi^0}\right]^3\left[\left[\frac{1}{3}\right]^{1/2}\frac{f_\pi}{f_{\eta_8}}\cos\Theta-2\left[\frac{2}{3}\right]^{1/2}\frac{f_\pi}{f_{\eta_1}}\sin\Theta\right]^2 ,\\ \frac{\Gamma(\eta'\to\gamma\gamma)}{\Gamma(\pi^0\to\gamma\gamma)}&=\left[\frac{m_{\eta'}}{m_\pi^0}\right]^3\left[\left[\frac{1}{3}\right]^{1/2}\frac{f_\pi}{f_{\eta_8}}\sin\Theta+2\left[\frac{2}{3}\right]^{1/2}\frac{f_\pi}{f_{\eta_1}}\cos\Theta\right]^2 ,\end{aligned} \tag{6.5}$$

where chiral-symmetry arguments[35] indicate that $f_\pi/f_{\eta_8}=0.8$. The mixing angle Θ can then be calculated with Eqs. (6.5) from the measured widths under several assumptions.

(1) In the case of all couplings being equal [condition (6.4)] the second of Eqs. (6.5) gives $\Theta=-21.5°$ $\pm2.3°\pm3.2°$.

(2) Assuming that $f_\pi=f_{\eta_8}$ gives [with both Eqs. (6.5)] $\Theta=-17.1°\pm1.2°\pm1.7°$ and $f_\pi/f_{\eta_1}=0.947\pm0.026$ ±0.040.

(3) If we take $f_\pi/f_{\eta_8}=0.8$, then $\Theta=-21.4°\pm1.2°$ $\pm1.7°$ and $f_\pi/f_{\eta_1}=0.971\pm0.026\pm0.039$.

These values of the mixing angle generally agree with other measurements in hadronic interactions and in ψ decays.

In QCD, gluonic bound states can also be expected to mix with quark-antiquark bound states. Such gluonic mixing may be present in the η and η' and has been discussed by Rosner[36] who assumes that the η and η' bound states are mixtures of gluon-gluon bound states and quark-antiquark states. The gluons, having no electric charge, do not couple to two photons, so the two-photon width is affected by the degree of gluon mixing. Rosner parametrizes this possible mixing with quark basis states as

$$\begin{aligned}|N\rangle&\equiv\frac{1}{\sqrt{2}}|u\bar{u}+d\bar{d}\rangle \ ,\\ |S\rangle&\equiv|s\bar{s}\rangle \ ,\\ |G\rangle&\equiv|\text{gluonium}\rangle \ ,\end{aligned} \tag{6.6}$$

$$|\eta\rangle=X_\eta|N\rangle+Y_\eta|S\rangle+Z_\eta|G\rangle \ , \tag{6.7}$$

$$|\eta'\rangle=X_{\eta'}|N\rangle+Y_{\eta'}|S\rangle+Z_{\eta'}|G\rangle \ , \tag{6.8}$$

$$X^2+Y^2+Z^2=1 \ . \tag{6.9}$$

The ratio of the two-photon widths of the η and η' to the two-photon width of the π^0 can then be written as

$$\frac{\Gamma(\eta\to\gamma\gamma)}{\Gamma(\pi^0\to\gamma\gamma)}=\frac{1}{9}\left[\frac{m_\eta}{m_{\pi^0}}\right]^3(5X_\eta+\sqrt{2}Y_\eta)^2 \ , \tag{6.10}$$

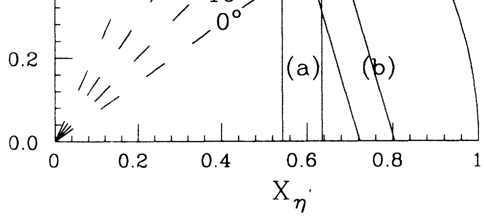

FIG. 21. Constraints on nonstrange ($X_{\eta'}$) and strange ($Y_{\eta'}$) quarkonium mixing coefficients in the η'. The circular arcs denote a pure quarkonium η'. The dashed lines from the origin give the corresponding mixing angle Θ for points in the $X_{\eta'}$-$Y_{\eta'}$ plane. (a) is the region allowed by $\Gamma(\eta'\to\rho\gamma)/\Gamma(\omega\to\pi^0\gamma)$. (b) is the region allowed by $\Gamma(\eta'\to\gamma\gamma)/\Gamma(\pi^0\to\gamma\gamma)$.

$$\frac{\Gamma(\eta'\to\gamma\gamma)}{\Gamma(\pi^0\to\gamma\gamma)}=\frac{1}{9}\left[\frac{m_{\eta'}}{m_{\pi^0}}\right]^3(5X'_\eta+\sqrt{2}Y'_\eta)^2 \, .$$

Equations (6.10) constrain the region of the X-Y parameter plane within which the actual values of X and Y for the η and η' can lie. Additional constraints on the allowed X-Y regions come from measurements of other decay widths. In particular

$$\frac{\Gamma(\eta'\to\rho\gamma)}{\Gamma(\omega\to\pi^0\gamma)}=3\left[\frac{m_{\eta'}^2-m_\rho^2}{m_\omega^2-m_{\pi^0}^2}\frac{m_\omega}{m_{\eta'}}\right]^3X_{\eta'}^2 \, . \qquad (6.11)$$

Figure 21 shows the regions of the $X_{\eta'}$-$Y_{\eta'}$ allowed by the equations (6.10) and (6.11), calculated using the most recent values of masses and partial widths and the average $\Gamma_{\eta'\to\gamma\gamma}$ measured in this paper. The allowed regions are consistent with no gluonium mixing in the η'.

ACKNOWLEDGMENTS

This work was supported in part by the U. S. Department of Energy under Contracts Nos. DE-AC0376SF00098, DE-AC0376SF00515, and DE-AC0276ER03064.

APPENDIX: THE HARDWARE TRIGGER EFFICIENCY CORRECTION

Following a primary trigger, the primary electronics sent a signal to MIC that in turn issued a WAIT flag halting data collection. The secondary trigger track-finding cycle was initiated by a simultaneous START pulse from the primary trigger. The master clock (MC) received the START signal, sent a BUSY flag to MIC, and oversaw the operation of the track-finding microprocessors at 10 MHz for 34 μsec. A deadtime of about 3% per kHz of primary trigger rate resulted from the MC cycle delay. The MIC received all secondary trigger data, from the track-finding electronics as well as from electronics associated with detector components other than the drift chambers, and arbitrated the final trigger decision.

The criteria used by MIC for selecting events to be logged were easily programmable on line, and several trigger formats were used during the experiment to accommodate short-term hardware problems, PEP running conditions, and test modes using cosmic rays. If a secondary trigger passed, MIC would interrupt the Mark II Vax 11/780 computer to initiate data transfer and subsequent logging to tape. The process was completed by MIC, whether or not a secondary trigger had occurred, by the lifting of the WAIT flag, and a system RESET.

A selected subset of 12 of the 24 logical OR's from all of the tracking layers plus the TOF system were available to the secondary trigger, and were used to define two types of legal tracks.

(1) *A tracks:* Those tracks passing through the entire tracking system, required typically 2 of 4 inner vertex-chamber (VC) layers hit, 4 of 8 selected drift-chamber (DC) layers hit where 2 of these 4 hits were in the outer 6 DC layers, and a TOF hit.

(2) *B tracks:* More steeply dipped tracks are called *B* tracks and usually only required 3 of 4 inner VC hits.

These two track categories are not mutually exclusive; most *A* tracks also satisfy the *B*-track requirements. The layers included in the trigger were changed occasionally: the outermost layer was removed from the trigger when its efficiency was seen to deteriorate, and during periods of high PEP beam noise it was sometimes necessary to remove a few inner VC layers to reduce excessive trigger rates.

The secondary trigger track finding was based on the mapping of the twelve trigger layers into shift registers which were then fed into specialized coincidence modules called curvature modules. A device known as the test and pickoff module transferred the tracking chamber shift register bits onto a dedicated trigger system bus. Twenty-four programmable curvature modules were tied to this dataway, to allow for two sets of twelve different coincidence masks, one for each sigma (clockwise or counterclockwise) of track curvature. The master clock provided 10-MHz clock pulses that served to rotate each shift register layer at a constant angular speed while the 24 curvature modules operated in parallel. Track counters were used to tally the results of the search, and to forward these results to MIC for a final secondary trigger decision. A block diagram of the track-finding system is given in Fig. 2.

The Monte Carlo program does not do an adequate job of simulating the hardware trigger for tracks with low transverse momentum relative to the beam line.

For an event to pass the Monte Carlo trigger and have a full simulation done for the event it is only necessary that one "*A* track" be found by its rough trigger simulation. Since the real hardware trigger usually requires two *A* tracks, and since we do not use events with tracks with transverse momentum less than 90 MeV/c and since the single track Monte Carlo trigger efficiency is 90%, the trigger efficiency for Monte Carlo two track events is at least 99%.

To correctly simulate the hardware trigger, real four-prong events were used to measure the trigger efficiency

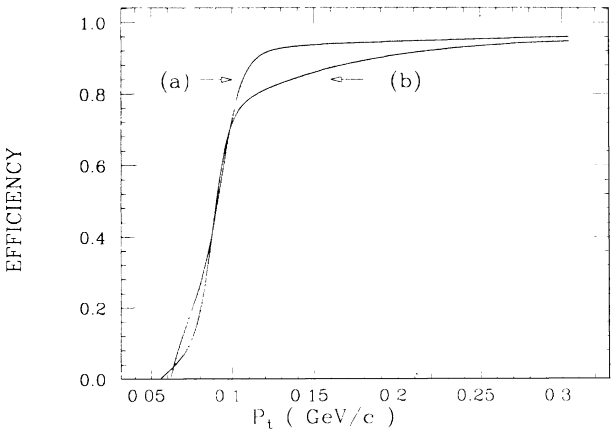

FIG. 22. Trigger efficiency of single tracks vs track P_t for (a) two prongs and (b) four prongs.

for single tracks by looking at the stored trigger information.

After a track vertex position cut we looked at events where tracks other than the one being considered cause the trigger to be satisfied. We could then look at the track being considered and use the stored hardware trigger information to decide if this track also triggered. The trigger efficiency was thus found as a function of the P_t and is shown in Fig. 22.

To correct the Monte Carlo events for trigger efficiency the parameters found by fitting the single-track efficiency were used to define an efficiency function, which was then applied to the Monte Carlo events. Note that the trigger efficiency at low momenta is strongly dependent on the vertex position cuts used to measure the efficiency. For this reason the trigger efficiency function used to correct the Monte Carlo calculation was separately found for each η' decay mode.

For the two-prong decays the trigger efficiency is simply the product of the two single-track trigger efficiencies, because two tracks are required to trigger for the event. For the four-prong decay $\eta' \to \eta\pi^+\pi^-$; $\eta \to \pi^+\pi^-\pi^0$, $\pi^+\pi^-\gamma$ the situation is considerably more complex, since 2, 3, or 4 tracks can have directions that will allow them to be classified as an "A track" by the trigger hardware logic.

For the four-prong case the trigger efficiency is then found by finding the total probability to trigger for the given set of tracks accounting for all combinations of single-track triggers that can satisfy the overall trigger. Not all the tracks make a large enough angle with the beam axis to help satisfy the trigger. The fitting error for each track combination is used to find the total error in the total trigger efficiency for the event.

By finding the single-track efficiency for charged tracks using a variety of selection criteria it became evident that the vertex position selection had the largest effect on the low P_t trigger efficiency. The nominal vertex position cut used for the $\eta' \to \rho\gamma$ and $\eta' \to \eta\pi^+\pi^-$; $\eta \to \gamma\gamma$ requires that the primary vertex constrained fit for each track's vertex position have a radius less than 1 cm and a Z position (position along the beam line) of -5 to 3.5 cm. For the decay mode $\eta' \to \eta\pi^+\pi^-$; $\eta \to \pi^+\pi^-\pi^0$, $\pi^+\pi^-\gamma$ the nominal vertex position selection was relaxed. The nonprimary vertex constrained vertex position must have a radius from the beam line of less than 5 cm and a Z position distance relative to the beam crossing point of less than 50 cm.

---

[a] Present address: University of Oklahoma, Norman, OK 73019.

[b] Present address: Columbia University, New York, NY 10027.

[c] Present address: University of Chicago, Chicago, IL 60637.

[d] Present address: Harvard Univeristy, Cambridge, MA 02138.

[e] Present address: Therma-Wave Corp., Fremont, CA 94539.

[f] Present address: Brookhaven National Laboratory, Upton, NY 11973.

[g] Present address: Fermi National Laboratory, Batavia, IL 60510.

[h] Present address: California Institute of Technology, Pasadena, CA 91125.

[i] Present address: University of Illinois, Urbana, IL 61801.

[j] Present address: CERN, CH-1211, Geneva 23, Switzerland.

[k] Present address: University of California, Santa Cruz, CA 95064.

[l] Present address: University of Pennsylvania, Philadelphia, PA 19104.

[m] Present address: Carleton University, Ottawa, Ontario, Canada, K1S 5B6.

[n] Present address: University of Florida, Gainesville, FL 32611.

[p] Present address: University of Geneva, CH-1211, Geneva 4, Switzerland.

[1] Mark II Collaboration, G. S. Abrams *et al.*, Phys. Rev. Lett. **43**, 477 (1979); P. Jenni *et al.*, Phys. Rev. D **27**, 1031 (1983).

[2] JADE Collaboration, W. Bartel *et al.*, Phys. Lett. **113B**, 190 (1982).

[3] CELLO Collaboration, H. J. Behrend *et al.*, Phys. Lett. **114B**, 378 (1982); **125B**, 518(E) (1983).

[4] PLUTO Collaboration, Ch. Berger *et al.*, Phys. Lett. **142B**, 125 (1984).

[5] TASSO Collaboration, M. Althoff *et al.*, Phys. Lett. **147B**, 487 (1984).

[6] JADE Collaboration, W. Bartel *et al.*, Phys. Lett. **160B**, 421 (1985).

[7] Stephen T. Lowe, in *Probing the Standard Model*, proceedings of the 14th SLAC Summer Institute on Particle Physics, Stanford, California, 1986, edited by E. C. Brennan (SLAC Report No. 312, Stanford, 1987).

[8] TPC/2γ Collaboration, H. Aihara *et al.*, Phys. Rev. D **35**, 2650 (1987).

[9] ARGUS Collaboration, H. Albrecht *et al.*, Phys. Lett. B **199**, 457 (1987).

[10] Crystal Ball Collaboration, D. Antreasyan *et al.*, Phys. Rev. D **36**, 2633 (1987).

[11] Preliminary versions of these measurements have appeared in *Photon-Photon Collisions*, proceedings of the Seventh-International Workshop, Paris, France, 1986, edited by A. Courau and P. Kessler (World Scientific, Singapore, 1987); in *Photon-Photon Collisions*, proceedings of the Eighth International Workshop, Shoresh, Israel, 1988, edited by U. Karshon (World Scientific, Singapore, 1988). This paper is based on a thesis submitted by Frederick Butler in partial fulfillment of the requirements for the Degree of Doctor of Philosophy, University of California, Berkeley, 1988.

[12] R. H. Schindler *et al.*, Phys. Rev. D **24**, 78 (1981); J. Jaros, in *Proceedings of the International Conference on Instrumentation for Colliding Beam Physics*, Stanford, California, 1982, edited by W. W. Ash (SLAC Report No. 250, Stanford, 1982).

[13] A. Roussarie *et al.*, Phys. Lett. **105B**, 82 (1982); J. R. Smith, Ph.D. thesis, University of California at Davis, 1983 (unpublished).

[14] Alan Rittenberg, LBL, Berkeley Report No. UCRL-18863 (unpublished).

[15] J. D. Jackson, Nuovo Cimento **34**, 1644 (1964).

[16] B. Muryn *et al.*, in *Photon-Photon Collisions*, proceedings of the VIII International Workshop, Shoresh, Israel, 1988, edited by U. Karshon (World Scientific, Singapore, 1988).

[17] M. Feindt, in *Glueballs, Hybrids, and Exotic Hadrons*, proceedings of the BNL Workshop, Upton, New York, 1988, edited by S-U. Chung (AIP Conf. Proc. No. 185) (AIP, New York, 1989).

[18] Nigel Lockyer, internal Mark II memo, 1984 (unpublished).

[19] Peter C. Rowson, Phys. Rev. Lett. **54**, 2580 (1985); LBL Report No. LBL-20463, Ph.D. thesis, 1985.

[20] J. H. Field, Nucl. Phys. **B168**, 477 (1980); **B176**, 545(E) (1980).

[21] The original thesis of F. Butler (LBL-26465) omits this correction and so the radiative widths given therein must be divided by 1.14.

[22] This supersedes a previous measurement of 4.7±0.6±0.9 given by G. Gidal *et al.*, Phys. Rev. Lett. **59**, 2012 (1987).

[23] The world average is dominated by the ARGUS result, without which it increases to 4.63±0.13 keV, in excellent agreement with our measurement.

[24] Particle Data Group, G. P. Yost *et al.*, Phys. Lett. B **204**, 1 (1988).

[25] Crystal Ball Collaboration, C. Edwards *et al.*, Phys. Lett. **110B**, 82 (1982).

[26] CELLO Collaboration, H. J. Behrend *et al.*, Phys. Lett. **114B**, 378 (1982); **125B**, 518(E) (1983).

[27] JADE Collaboration, J. E. Olsson, in *Photon Photon Collisions,* proceedings of the Fifth International Workshop on Photon Photon Collisions, Aachen, Germany, 1983, edited by C. Berger (Lecture Notes in Physics, Vol. 191) (Springer, Berlin, 1983), p. 45.

[28] PLUTO Collaboration, Ch. Berger *et al.*, Phys. Lett. **149B**, 427 (1984).

[29] Crystal Ball Collaboration, D. Antreasyan *et al.*, Phys. Rev. D **33**, 1847 (1986).

[30] TASSO Collaboration, M. Althoff *et al.*, Z. Phys. C **31**, 537 (1986).

[31] TCP/2γ Collaboration, H. Aihara *et al.*, in *Proceedings of the International Europhysics Conference on High Energy Physics,* Uppsala, Sweden, 1987, edited by O. Botner (European Physical Society, Petit-Lancy, Switzerland, 1987).

[32] Particle Data Group (Ref. 24); H. W. Atherton *et al.*, Phys. Lett. **158B**, 81 (1985).

[33] M. Chanowitz, in *Proceedings of the VIth International Workshop on Photon-Photon Collisions,* Lake Tahoe, California, 1984, edited by R. L. Lander (World Scientific, Singapore, 1985).

[34] F. Gilman and R. Kauffman, Phys. Rev. D **36**, 2761 (1987).

[35] J. Donoghue, B. Holstein, and Y. Lin, Phys. Rev. Lett. **55**, 2766 (1985); J. Gasser and H. Leutwyler, Nucl. Phys. **B250**, 465 (1985).

[36] J. L. Rosner, Phys. Rev. D **27**, 1101 (1983).